

Bending and Rolling Shear Properties of Cross-Laminated Timber Fabricated with Canadian Hemlock

Gengmu Ruan¹, Haibei Xiong^{1,*} and Jiawei Chen¹

Abstract: In this paper, bending performance and rolling shear properties of cross-laminated timber (CLT) panels made from Canadian hemlock were investigated by varied approaches. Firstly, three groups of bending tests of three-layer CLT panels with different spans were carried out. Different failure modes were obtained: bending failure, rolling shear failure, bonding line failure, local failure of the outer layer and mixed failure mode. Deflection and strain measurements were employed to calculate the global and local modulus of elastic (MOE), compared with the theoretical value. In addition, a modified compression shear testing method was introduced to evaluate the rolling shear strength and modulus, compared with the results from strain measurements in bending shear tests. According to testing results, bonding line failure and rolling shear failure were dominant failure modes in bending tests, and the theoretical value of bending property was beyond the average level of the calculating results obtained from both deflection and strain measurements. In addition, the rolling shear strength and modulus obtained from compression shear tests were relatively smaller than those from bending tests.

Keywords: Bending properties, rolling shear properties, failure modes, bonding line.

1 Introduction

Currently, cross-laminated timber (CLT) that originated from Germany and Austria in the early 1990s, is undoubtedly the most popular timber construction product worldwide because of its excellent mechanical properties and environmentally friendly performance [Karacabevli and Douglas (2013)]. The needs of CLT production dramatically raised in recent years, because of the increasing number of CLT applications. However, the CLT production in China is extremely limited, due to the poor forestry resources and less CLT manufacturers. In order to decrease the emissions of carbon and to promote the development of prefabricated buildings, local CLT producers are officially encouraged to import raw materials abroad and manufacture the CLT elements locally to satisfy the needs of Chinese construction market.

Above all, it is essential to figure out the mechanical property of CLT which is made from foreign species before construction applications. As CLT panels are usually served as floors and walls, the bending properties of CLT panels are the basic considerations and criterions of the structural design. EN 16351 [CEN (2015)], EN 408 [CEN (2012)] and

¹ College of Civil Engineering, Tongji University, Shanghai, 200092, China.

* Corresponding Author: Haibei Xiong. Email: xionghaibei@tongji.edu.cn.

ASTM D198 [ASTM (2015)] both recommend a four-point bending test method with variable lengths of span to evaluate the bending property of CLT panels. In some cases, this method was adopted to investigate the bending property of CLT panels made from different species. A group of four-point bending tests with the span-to-depth ratio of 27:1 was conducted [Hindman and Bouldin (2015)] to test the bending property of CLT fabricated with southern pine, comparing to the ratio of 30:1 specified by PRG 320 [ANSI/APA (2018)]. The results indicated that the bending strength and stiffness met or exceeded the requirements of the V3 grade CLT defined in ANSI/APA [ANSI/APA (2018)]. Some four-point bending tests of three-layer and five-layer CLT panels with loading in the out-of-plane and in-plane directions were carried out to investigate the effect of the thickness of CLT panel on bending stiffness and strength [Sikora, McPolin and Hart (2016)]. A raising tendency was found in the bending strength with the increasing thickness of the panel. Four configurations of three-layer CLT fabricated with laminated strand lumber (LSL) or/and Spruce-Pine-Fir (SPF) were employed in the four-point bending tests in Davids et al. [Davids, Willey, Lopez-Anido et al. (2017)], to evaluate the bending performance of hybrid CLT panels. The results indicated that a low-grade LSL core in hybrid panels could clearly increase the strength of CLT panels. Steiger et al. [Steiger, Gülzow, Czaderski et al. (2011)] compared bending stiffness of CLT derived by modal analysis and four-point bending tests, a width of 300 mm was indicated as good accuracy of testing the stiffness properties.

However, the bending property is not the only considered factor in bending tests, especially when testing beams or panels are relatively short. The most normal failure mode in such a situation is rolling shear failure in the cross-layer [Aicher and Dill-Langer (2001); Bendsten (1976)]. The main reason is that the shear strength and modulus of the cross layer is weak (in Tangential and Radial (TR) plane), and when the shear force is relatively high (Span-to-height is small), the rolling shear failure may occur, as shown in Fig. 1. Therefore, rolling shear strength and modulus of the cross-layer have been identified as a key issue in CLT panels for out-of-plane bending applications [Blaß and Görlacher (2000)]. Rolling shear properties of CLT mainly depend on species, cross-layer density, laminate, thickness, moisture content, sawing pattern configurations (annual rings orientation), size and geometry of the panel's cross-section. Some methods in Europe have been developed to measure the rolling shear properties of CLT, such as a non-destructive evaluation method [Steiger, Gülzow and Gsell (2008)].

However, there is not a universe standardized test method for the determination of rolling shear properties of full-size CLT panels. Some methods, such as the varied-span bending method and the compression shear testing method, were recommended in Europe [CEN (2015); CEN (2012)] and North America [ASTM (2011)]. The compression shear test was employed in many research cases to investigate rolling shear properties of CLT. Some European timber species were tested to investigate the potential influencing parameters, including density, sawing pattern, board geometry and species, on rolling shear properties [Ehrhart, Brandner, Schickhofer et al. (2015)]. Totally more than 200 tests were conducted to prove that the test figuration of compression was functional and sawing pattern and board geometry were the main influencing parameters of rolling shear properties. The compression shear testing method was recommended as a standardized testing method for measuring the rolling shear modulus after testing three-layer CLT

made from black spruce by using central-point bending tests and compression shear tests. [Zhou, Gong, Chui et al. (2014)] A good prediction of deflections of CLT beams using shear analogy method based on the compression shear test could be obtained when the span-to-depth ratio is around 20.

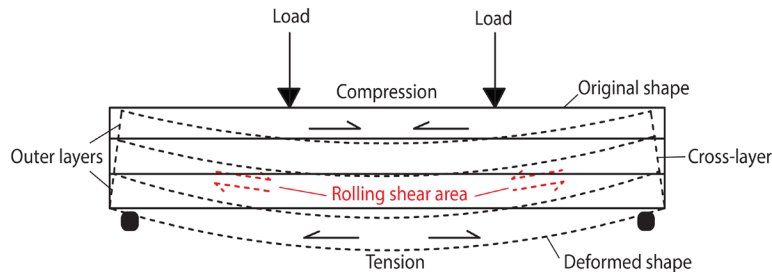


Figure 1: Rolling shear area in bending tests of cross-laminated timber

Besides, some modified compression shear tests were adopted to measure rolling shear properties. A new type of modified compression shear test was employed to evaluate rolling shear properties of hybrid CLT fabricated with lumber and laminated veneer lumber (LVL) [Wang, Fu, Gong et al. (2017)]. It was proved that SPF dimension lumber had higher rolling shear properties than LVL panels. Another type of modified methods was performed in investigations on CLT made from Radiata pine, compared with the results from varied-span bending tests [Li (2017)]. A relatively high rolling shear strength was obtained from the varied-span bending test because relatively high compressive stresses perpendicular to fiber may be introduced in cross-layers thus affecting the evaluation of rolling shear strength.

Apart from the compression shear testing method, rolling shear properties also could be calculated by theoretical methods, including gamma method (γ -method), composite method (k-method) and shear analogy method [Kreuzinger (1999); Blass and Fellmoser (2004)]. For instance, stress and strain measurements in the cross-layer areas of bending specimens were conducted to compute rolling shear modulus by using shear analogy method [Aicher, Hirsch and Christian (2016)]. However, rolling shear strength and modulus are influenced by the size effects which cause a larger result from the calculating value of bending tests than that from compression shear tests [Li (2015)]. The detailed relationship of the results obtained from two methods is unknown.

In this paper, Canadian hemlock CLT panels imported abroad and manufactured by a local CLT producer were introduced. In order to explore its bending performance, three groups of three-layer CLT panels with different spans were designed for four-point bending tests. The results of bending tests measured by various approaches were compared with a theoretical value. In addition, a new modified compression shear test was hired to investigate rolling shear properties, and the results were compared with the calculating value from strain measurements in bending tests. Both bending and rolling shear properties of CLT panels made from Canadian hemlock were explored by different approaches, and the relationship between the results calculated by strain and deflection measurements were discussed.

2 Materials and methods

2.1 Test materials

The raw material for the outer and cross-layer of CLT panels was Canadian hemlock with no finger joints. The industrial manufacture of the three-layered full-scale CLT panels was performed in a local CLT producer (Ningbo Sino-Canada Technology Research Institute, Zhejiang, China). Before panel fabrications, timber boards were kiln-dried to a moisture content (MC) of approximately 12%, stored in a limited indoor condition of 40% R.H. and 10°C. The measurements of density of the boards ranged from 500 kg/m³ to 600 kg/m³. In material property tests, the modulus of elastic (MOE) parallel and perpendicular to the grain was recorded with a mean value of 10766.5 N/mm² and 978.5 N/mm² respectively. Each board was cut into the same width of 140 mm and thickness of 35 mm, preparing for CLT panel fabrications.

The panels were planed to 5.4 m long (paralleled to the outer layers) and 1.2 m wide (paralleled to the cross-layer) before cutting into the designed dimensions. The thickness of each layer was 35 mm and hence the depth (h) of three-layer CLT panel was 105 mm. The face bonding of each layer was performed with a PUR adhesive, produced by H.B. Fuller Company. After uniformly spreading the PUR adhesive between each layer, boards were pressed by a hydraulic press device with a clamping pressure of 9 N/mm² for 45 minutes. After clamping, the boards were placed in the plant, separated by several wood supports in between, as seen in Fig. 2.



Figure 2: CLT panels stored in the plant

2.2 Test setup, specimens and procedure

2.2.1 Bending tests

The load configurations were in accordance with EN 16351 and EN 408, which recommended a four-point bending over a span of 18 or 24 times the thickness (h) for bending strength and stiffness determination perpendicular to plane and a four-point bending over a span of 12 times the thickness for rolling shear strength and stiffness determination perpendicular to plane. The width of all specimens was 300 mm, recommended by Steiger et al. [Steiger, Gülzow, Czaderski et al. (2011)]. The distance between two loading points was $6h$ for all configurations and the distance between loading point and the central line of supports was either $3h$, $6h$ or $9h$. Therefore, the spans of three specimen groups were planned as $12h$, $18h$ and $24h$, which were labelled as

group L1, L2 and L3. All the test specimens and sizes are shown in Tab. 1. The panels were simply supported during the tests, and loads were applied cross the whole width of CLT specimens by using steel rollers. To make sure that, the width of steel plate was designed slightly wider than the width of CLT panel and central symmetry to the panels. All tests were performed in a servo-hydraulic test machine (CELTRON PSD-20tSJTT) which was fixed to the reaction frame. The loading was displacement-controlled at a constant rate of 6.0 mm/min to ensure that the maximum load reached within (300±120) s. The realized testing device was shown in Fig. 3(a).

Table 1: Sizes and determined properties of CLT panels

Spec. No.	Thickness h (mm)	Width b (mm)	Span in bending l (mm)	Shear area length a (mm)	Determined properties
L1-1	105	300	1260	315	Bending strength & stiffness
L1-2					
L1-3					
L1-4					
L1-5					
L1-6					
L2-1	1890	630	2520	945	
L2-2					
L2-3					
L3-1					
L3-2					
L3-3					

Tests were carried out in two stages. Initially, a pre-load of 5 kN was applied to eliminate the influence of the gaps between bolts and steel plates in the loading device, ensuring that the starting point of displacement was zero. In the second stage, the load was directly applied to the ultimate value, and then to the capacity-losing state. The testing was immediately ended when the load suddenly fell down to a relatively low value or the failure of specimens can be visually distinguished.

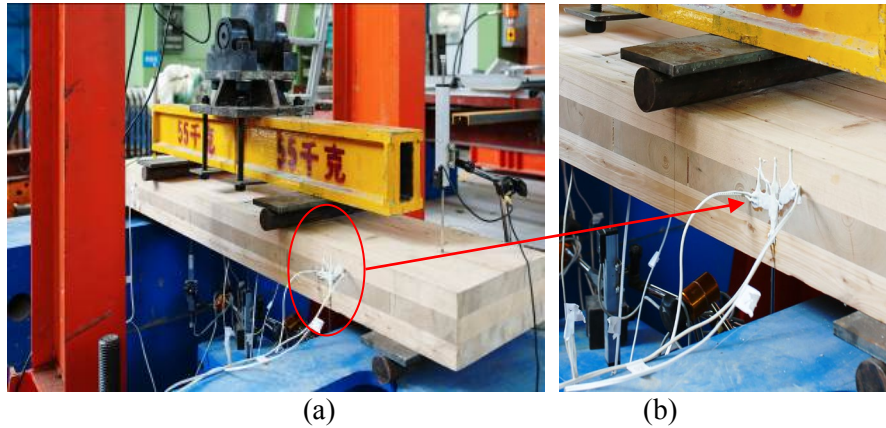


Figure 3: Realized testing setup: (a) bending tests setup; (b) strain measurement in bending tests for the determination of rolling shear property

2.2.2 Deflection and strain measurements in bending tests

The deflection of all specimens was measured globally at the middle of the span and locally at the middle-span over a length of $l_1=6h$ within the pure bending zone. The global deflection, w_{global} , was calculated as the displacement at the middle of the span plus the mean displacement of the support; the local deflection, w_{local} , was calculated as the displacement at the middle of the span minus the mean displacement at the loading point. Therefore, five linear variable differential transformers (LVDT) with the range of ± 100 mm was arranged at the middle-width ($\pm b/2$) of the different positions of the specimens (middle-span, loading points and the central line of supports). The details of the arrangements of deflection measurements are shown in Fig. 4.

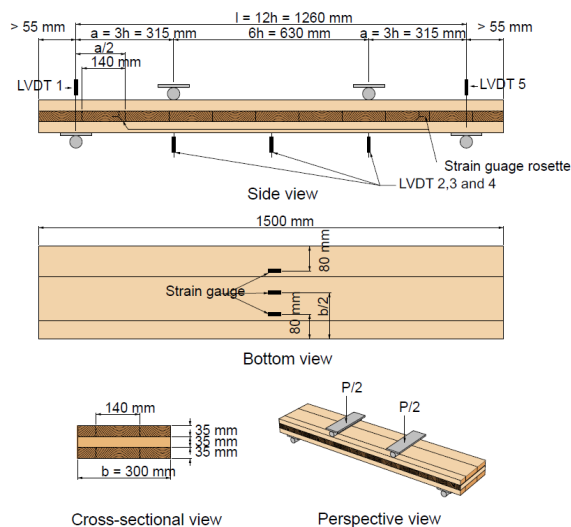
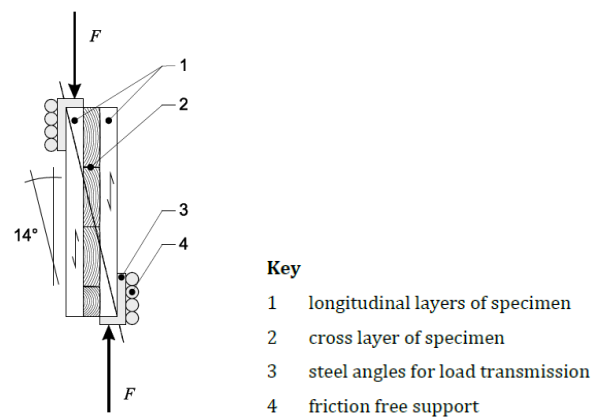


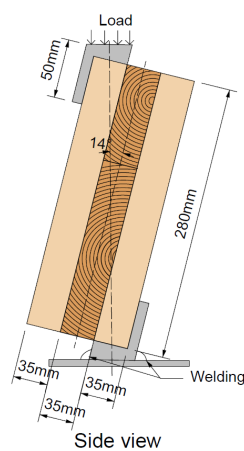
Figure 4: Test scheme, specimen dimensions and deflection and strain measurement locations of bending tests (L1)

Three strain gauges were applied at the middle span of outer layer on the bending tension side to measure the MOE paralleled to fiber. The gauge lengths of strain gauge rosettes and strain gauges were both 10 mm, connected to a quarter bridge circuit. All the test arrangements of L1 are shown in Fig. 4. The measurement setup for determination of MOE and bending strength of group L2 and L3 was similar with group L1, apart from the lengths of the shear constant area ($6h$ of group L2 and $9h$ of group L3).

In order to collect the data for the calculation of rolling shear strength and modulus, strain gauge rosettes were fixed at the middle of the shear constant area in both sides, to measure the shear strain of the cross-layer, as shown in Fig. 3(b). The strain gauge rosettes were installed at least 20 mm away from the gap between two elements in the cross-layer, as well as knots, to avoid the influence on the measurements of strains.



(a)



(b)

Figure 5: Test configurations: (a) the recommendation in EN 16351; (b) the adopted modified configuration in the real test

A newly modified testing setup was adopted here, according to the testing method recommended in EN 16351 which recommends a test configuration loaded in vertical direction (Fig. 5(a)). Totally 12 compression shear specimens were cut from the same batch of CLT boards in a same dimension (length $l_c=280$ mm, width $b_c=100$ mm and thickness $t_c=105$ mm). Two steel wedge were manufactured to adjust the specimens to a certain angle 14° ($\tan 14^\circ \approx 1/4$). One steel wedge on the top was connected to the loading end, in order to transfer the load to the one narrow edge of the outer layer of compression shear specimens. Another wedge was welded to a steel plate which was fixed on the ground, in order to limit both the lateral and the vertical displacement during the test. Two LVDTs were arranged at both sides of the specimens to calculate the displacements of the loading parallel to the outer layer fiber. A hydraulic jack (SYB-4, Shanghai Hengyi Hydraulic Device Limited company) was hired to exert loads to the compression shear specimens, and a sensor with measuring range of 100 kN was employed to collect the data of loads. LTDVs were connected to the same sensor to record the displacement information. The detailed dimensions and realized device are shown in Fig. 5(b).

3 Results and discussion

3.1 Bending tests

3.1.1 Ultimate loads and failure modes of group L1

In group L1 of bending tests, the global load-middle span deflection curves of all specimens are strictly linear up to about 60-70% of the ultimate load F_u . The load-deflection curves of all specimens in group L1 are shown in Fig. 6(a). The whole loading process of each specimen is given, in which the straight line of dramatically falling down after rupture failure represents the loads are removed. According to the load-deflection graph, a potential of good ductility of the bending specimens with a span length of $12h$ is indicated.

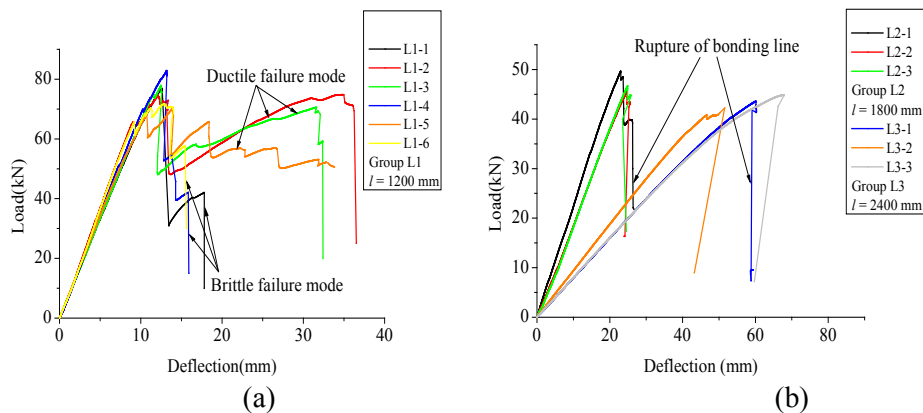


Figure 6: Load-deflection curve: (a) group L1; (b) group L2 and L3

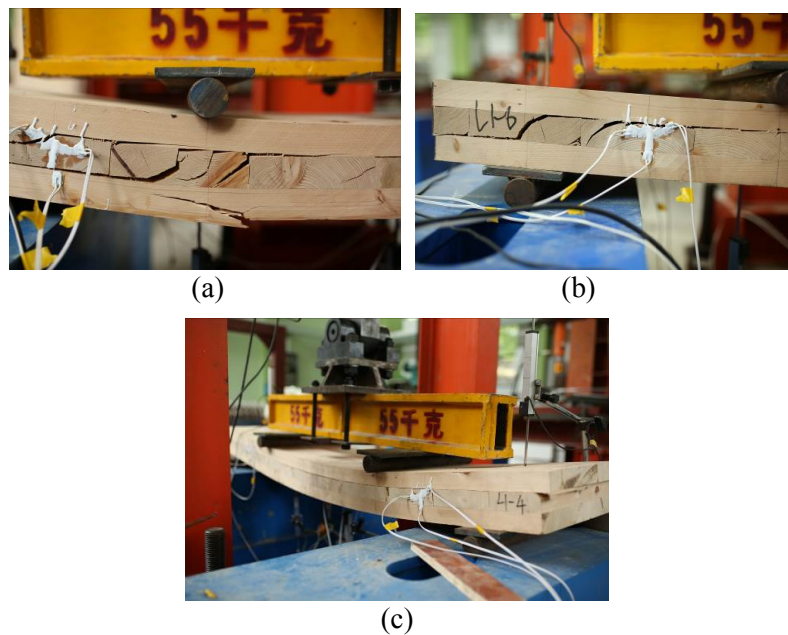


Figure 7: Failure modes in group L1: (a) rolling shear and bending failure; (b) rolling shear and bonding failure and (c) bonding failure

Some specimens (L1-2, L1-3 and L1-5) performed a good load bearing capacity (60-70% F_u) after linearly reaching the peak load. The curve slowly climbs to a post-peak point after arriving the first peak point, then completely losing the bearing capacity at a relatively long distance from the original point (ranged from 50 mm to 70 mm). Even a higher value of the post-peak point is obtained in L1-2, which reaches 74.8 kN at the second peak point, compared with 74.6 kN at the first peak point. These specimens normally showed a mixed failure mode, combined the rolling shear failure mode of the cross-layer and the bending failure mode of the outer layer: At first, some slight cracks developed along with the directions of annual rings in the cross-layer before reaching the first peak load. Then, the rolling shear failure occurred at the middle area of the shear constant area when the load raised up to the first peak load. After reaching the first peak load, the cracks continued developing with the increasing deflections. At the end, the bending tension side of the outer layer suddenly broke when the load arrived the second peak point and the load dramatically fell down to a relatively low level. The final failure mode can be seen in Fig. 7(a).

In other cases of group L1 (L1-1, L1-4 and L1-6), the load-displacement curve is strictly linear up to about 70-80% of the ultimate load F_u , and then the load dramatically declines to 30-40% F_u after arriving the peak load (Fig. 7(a)), acting as the rupture of the wood fiber (a typical brittle failure mode). A mixed failure mode combined a rolling shear failure with a bonding line failure was expressed. In addition, the bonding line failure between the outer layer and the cross-layer happened in few cases. Both two failure modes showed a brittle bonding failure occurred at the first peak point and the only

difference is that no rolling shear failure occurred in the L1-4. The details of this failure mode are shown in Figs. 7(b) and 7(c).

3.1.2 Ultimate loads and failure modes of group L2 and L3

In group L2 and L3, the global load-middle span deflection curves are strictly linear up to approximately 90% of the F_u , as shown in Fig. 6(b). Different from the failure modes in group L1, a bonding line rupture failure simultaneously occurred with rolling shear failures was the dominant failure mode in group L2 and L3: During the loading process, some voices of fracture of the wood fiber could be clearly heard when the load was close to F_u . As the load arrived the ultimate load, the bonding line suddenly ruptured, accompany with the rolling shear failure occurred in the cross-layer elements. The details of this failure mode can be found in Figs. 8(a) and 8(b). However, a different failure mode was obtained in L3-3, performing as the rupture of the outer layer across the narrow section on the one side of the specimen (Fig. 8(c)), together with the fracture alongside the bonding line on the other narrow side (Fig. 8(d)). The main reason of this failure mode maybe that the moisture content of the outer layer on the bottom side is higher than that of other parts in the specimen L3-3, due to the influence of storage condition (The specimen was placed underground and was once soaked in the water in the weather condition of raining). When testing, the moisture content was control around 12%, so the wood shrunk and the strength of the local area decreased, leading to a local failure across the outer layer. However, L3-3 showed a similar strength with other specimens in group L3, which was even a bit higher. It indicated that the local shrinkage had a few influence on the strength but changed the failure mode locally.

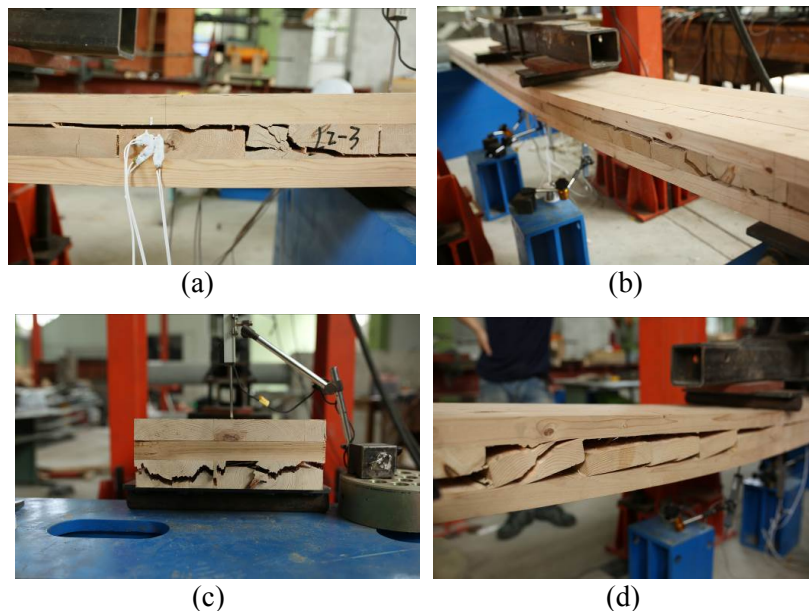


Figure 8: Failure modes in group L2 and L3: (a) (b) rolling shear and bonding failure; (c) outer layer rupture failure in L3-3 and (d) bonding failure in L3-3

3.1.3 Evaluation of bending properties

Two methods are adopted here to evaluate the MOE of the Canadian CLT panels. One is based on displacement measurements and another one is derived from strain measurements. In the first method, the value of local MOE ($E_{local,def}$) and global MOE ($E_{global,def}$) obtained from deflection measurements were calculated by using Eq. (1) and Eq. (2) respectively [3]. ‘global’ modulus is calculated by taking the shear modulus (G) as infinite and 500 N/mm² [CEN (2016)] considering whether taking the influence of shear deformations into consideration ($E_{global,def,500}$) or not ($E_{global,def,\infty}$). To make sure both forces and deflections are in elastic phase, F_2 and F_1 correspond to 10% and 40% of F_u , while ω_1 and ω_2 correspond to 10% and 40% of the ultimate deflection respectively.

$$E_{local,def} = \frac{al_1^2(F_2 - F_1)}{16I(\omega_2 - \omega_1)} \quad (1)$$

$$E_{global,def} = \frac{3al^2 - 4a^3}{4bh^3 \left(\frac{\omega_2 - \omega_1}{F_2 - F_1} - \frac{3a}{5Gbh} \right)} \quad (2)$$

Another method is to measure local MOE of the outer layer, adopted by collecting the data from the strain gauges on the surface of outer layer at the bending tension side. According to Eqs. (3) and (4), the value of local MOE ($E_{local,strain}$) is approximated by using the γ -method approach [CEN (2018)], in which σ_m represents the bending stress, and ε represents the bending strain obtained from the strain measurements. All results are performed in Tabs. 2 and 3.

$$E_{local,strain} = \frac{\sigma_m}{\varepsilon} \quad (3)$$

where

$$\sigma_m \approx \pm \frac{M}{I} \cdot \frac{3t}{2} \quad (4)$$

3.1.4 Evaluation of bending properties

The theoretical value (E_{Theo}) calculated by the Eq. (5) which is recommended in *CLT Handbook* [Karacabeyli and Douglas (2013)] is compared with all the calculated values.

$$E_{Theo} = \frac{1}{I} \sum_{i=1}^n \left(E_i \frac{b_i h_i^3}{12} + E_i b_i h_i z_i^2 \right) \quad (5)$$

The values of global and local MOE calculated by strain measurements and deflection measurements show varied levels in various lengths of span, as shown in Fig. 9. In calculated results, the average value of $E_{local,strain}$ is the largest one due to the fact that the local MOE only considers the local areas at the middle of the outer layer parallel to the fiber. The value is close to the result of clear wood property because of less existence of defects. On the contrary, the average calculated results of $E_{global,def,\infty}$ is the lowest one, it

may because it not only considers a global stiffness (combining outer layers and cross-layers), but also ignores the contribution of shear force.

In group L2 and L3, relatively low values of MOE measured by local deflections are performed. The large difference may be caused by more growth defects in the longer specimens, i.e., knots and worm holes. Especially in group L3, a large deviation of $E_{local,def}$ reflects the distinguishing extents of the influence of growth defects.

With the longer length of span, an increasing trend of global MOE is obtained, while local MOE calculated by strain measurements is identical with the theoretical value, and local MOE calculated by deformations is below the level of the theoretical results.

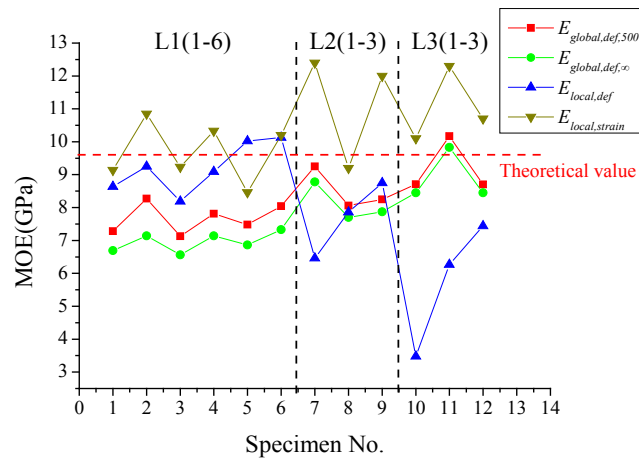


Figure 9: Comparison of the values of MOE obtained from different methods

3.2 Compression shear tests

3.2.1 Ultimate loads and failure modes in compression shear tests

In compression shear tests, failures in all 12 compression shear specimens finally occurred as bonding failure, combined with rolling shear failure in partial cases. In almost half cases, failures occurred alongside the bonding lines between outer layers and cross-layers, across the gaps between the adjacent unglued cross-layers, as shown in Fig. 10. The possible reason of the occurring of this failure mode is the low bonding strength of bonding lines. As a result, the specimens failed in this way were excluded from the calculation of rolling shear properties.

Other specimens which were performed as rolling shear failure mode in cross-layers were taken into account, accompany with the bonding failure between outer layers and the cross-layers, as seen in Fig. 11. Cracks in the cross-layers were typical with an angle of 45° through the cross-layer, originally starting or finally ending at the unglued narrow edges. In addition, the directions of cracks were either vertical to the annual rings or alongside with them, which indicated that the strength in these two directions was lower than other directions in the cross-layer. All these specimens performed as a ductile failure process: cracks occurred, cracks developed, cracks developed through the cross-layer with the bonding line breaking.

Table 2: Results obtained from bending tests (L1)

Spec.	Type of failure	Max. bending stress	Global MOE from global deflection			Local MOE	
No.	shear(rolling) /bending/ bonding failure	σ_m	$E_{global,def,500}$ $G=500 \text{ N/mm}^2$	$E_{global,def,\infty}$ $G=\infty$	from local deflection $E_{local,def}$	from strain measurement $E_{local,strain}$	<i>COV of</i> $E_{local,strain}$
-	-	(N/mm ²)	(kN/mm ²)	(kN/mm ²)	(kN/mm ²)	(kN/mm ²) Mean	-
L1-1	shear+bonding	21.97	7.28	6.69	8.64	9.14	5%
L1-2	shear+bending	21.26	8.27	7.14	9.25	10.85	0%
L1-3	shear+bending	22.24	7.13	6.56	8.19	9.23	3%
L1-4	bonding	23.69	7.81	7.14	9.09	10.33	19%
L1-5	shear+bending	20.08	7.48	6.86	10.02	8.46	5%
L1-6	shear+bonding	20.51	8.04	7.33	10.13	10.2	2%
Mean	-	21.63	7.67	6.95	9.22	9.7	-
SD	-	1.19	0.41	0.27	0.69	0.82	-
COV	-	6%	5%	4%	8%	8%	-

Table 3: Results obtained from bending tests (L2 and L3)

Spec.	Type of failure	Max. bending stress	Global MOE from global deflection			Local MOE	
No.	shear(rolling) /bending /bonding/outer layer failure	σ_m	$E_{global,def,500}$ $G=500 \text{ N/mm}^2$	$E_{global,def,\infty}$ $G=\infty$	from local deflection $E_{local,def}$	from strain measurement $E_{local,strain}$	<i>COV of</i> $E_{local,strain}$
-	-	(N/mm ²)	(kN/mm ²)	(kN/mm ²)	(kN/mm ²)	(kN/mm ²) Mean	-
L2-1	shear+bonding	28.15	9.25	8.78	6.46	12.4	5%
L2-2	bonding	26.49	8.06	7.7	7.86	9.2	12%
L2-3	shear+bonding	27.08	8.25	7.87	8.75	12	20%
Mean	-	27.24	8.52	8.12	7.69	11.2	-
SD	-	0.69	0.52	0.47	0.94	1.4	-
COV	-	3%	6%	6%	12%	13%	-
L3-1	shear+bonding	37.31	8.71	8.45	3.48	10.1	1%
L3-2	shear+bonding	36.15	10.17	9.83	6.27	12.3	5%
L3-3	bonding+local rupture in the outer layer	38.45	8.7	8.45	7.44	10.7	2%
Mean	-	37.3	9.19	8.91	5.73	11.03	-
SD	-	0.94	0.69	0.65	1.66	0.93	-
COV	-	3%	8%	7%	29%	8%	-

3.2.2 Calculation of rolling shear modulus and strength in compression shear tests

The rolling shear modulus (G_r) of the cross-layer was calculated using Eq. (6) where F/Δ represents the slope of the load-displacement curve of each specimen and α is 14° in this paper. l_c and b_c mean the length and width of compression shear specimen. The rolling shear strength (f_v) of the cross-layer is calculated using Eq. (7).

$$G_r = \frac{t_2}{l_c \times b_c} \times \frac{F}{\Delta} \times \cos \alpha \quad (6)$$

$$f_v = \frac{F_{\max}}{l_c \times b_c} \times \cos \alpha \quad (7)$$

All the results of compression shear specimens performed in rolling shear failure mode are summarized in the Tab. 4. The mean value of f_v and G_r are 1.28 MPa and 53.13 MPa, with the coefficients of variation (COV) of 15% and 36%, respectively. The main reason for the relative large difference of rolling shear modulus is that different sawn patterns are employed as the raw materials of cross-layers, which may cause the diversity of material properties, especially rolling shear properties. In addition, the growing defects are not uniformly distributed, which might also affect the rolling shear properties. For instance, the cross-layer of specimen RS3 was obtained from the sawn pattern far away the pith, showing a larger strength than specimen RS10 which was equipped with the pith part in the cross-layer.

Table 4: Rolling shear properties obtained from compression shear tests

Specimen. No.	Rolling shear strength f_v	Rolling shear modulus G_r	Failure mode
-	N/mm ²	N/mm ²	
RS2	1.24	88.22	rolling shear
RS3	1.09	39.05	
RS4	1.56	69.80	
RS5	1.07	37.65	
RS10	1.53	40.98	
RS12	1.16	43.05	
Mean	1.28	53.13	
SD	0.20	19.13	-
COV	15%	36%	-

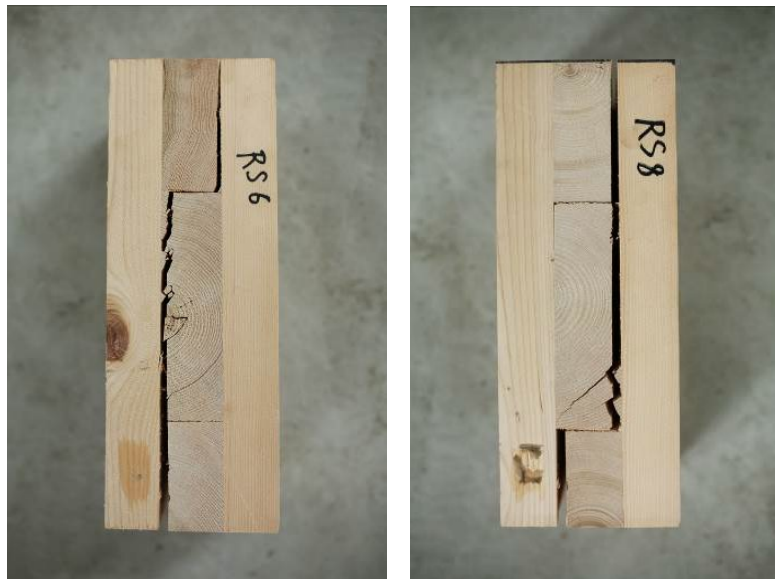


Figure 10: Bonding line failure in compression shear tests



Figure 11: Rolling shear failure in compression shear tests

3.2.3 Calculation of rolling shear modulus and strength in bending shear tests

Half of the bending shear specimens (L1-2, L1-3 and L1-5) performed as a typical rolling shear failure mode of the cross-layer in the shear constant area, as shown in Figs. 6(a) and 6(b). There are three specimens that failed with a ductile process because of the gradually developing cracks in the cross-layer, and finally failed when the crack developed across the cross-layer accompany with the fracture of the bonding line. It means that the shear

capacity of the cross-layer is utilized as much as possible before the failure of itself. The ultimate loads of the bending shear specimens were approximately 60-70 kN, and shear deformation-load curves of these specimens are shown in Fig. 12, which shows an approximate linear relationship up to 40-50% ultimate load. It indicates that the shear strains in the shear constant area are developed in elastic phase, and the measurements of strain rosette gauges are estimable. The average value of the shear strain of each specimen is close, even though the deviations from a few strain rosettes are relatively large because of few cracks occurred in the measuring area.

Based on the measuring results, a good approximate value of $\gamma/\eta \approx 1$ could be obtained due to the constant shear stress along the depth of cross-layers. The rolling shear modulus can be calculated as Eq. (8), which was recommended in Aicher et al. [Aicher, Hirsch and Christian (2016)], where $\tau_{r,2}$ means the rolling shear stress, $t_{1,3}$ and t_2 represent the thickness of the outer layer and the cross-layer respectively. The shear force V can be directly obtained from the loading device, while the data of rolling shear strains $\gamma_{r,2}$ are collected from strain rosettes. The rolling shear modulus ($G_{r,strain}$) can be calculated by using Eq. (9), where the highest value of $\tau_{r,2}$ is equal to the rolling shear strength $f_{v,r}$. The results of rolling shear modulus and strength of bending shear tests are shown in Tab. 5.

$$\tau_{r,2} \approx \frac{V\gamma t_{1,3}(t_{1,3} + t_2)}{2I\eta} = \frac{Vt^2}{3I} \quad (8)$$

$$G_{r,strain} = \frac{\tau_{r,2}}{\gamma_{r,2}} \quad (9)$$

Table 5: Rolling shear properties obtained from bending shear tests

Specimen	Rolling shear strength	Rolling shear modulus
No.	$f_{v,r}$	from strain measurement $G_{r,strain}$
-	(N/mm ²)	(N/mm ²) <i>Mean</i>
L1-2	1.57	248
L1-3	1.65	240
L1-5	1.49	213
Mean	1.57	234
SD	0.07	14.97
COV	4%	6%

3.2.4 Comparison and discussion of rolling shear properties between two methods

The average values of rolling shear strength obtained from compression shear tests and bending shear tests are 1.28 MPa and 1.57 MPa, respectively. The influential reasons for this discrepancy might be growing defects, sawn patterns or dimensions. However, the most possible reason which has an obvious impact on rolling shear strength is size effects [Madson and Buchannan (1986)]. Therefore, a larger value of rolling shear strength from bending shear tests is obtained, with an adjustment factor of 1.2 to that of compression shear

tests when the span-to-depth ratio is 12. It indicates that the compression shear test can be conservatively estimated for the rolling shear strength of Canadian hemlock CLT when the span is relatively short (rolling shear failure preforms as the dominate failure mode).

For determination of the rolling shear modulus, the results calculated by strain measurements at the edge of shear constant areas are more than four times of the value from compression shear tests (234 MPa and 53.13 MPa). Apparently, the rolling shear modulus of small compression shear specimens is much lower than that of a structural element. Apart from size effects, the possible reason for the large difference is that the adjacent parts of the testing area in bending shear specimens make large contributions to bearing shear loads while the specimen in the compression shear test has no “helpers”.

As a result, the rolling shear strength measured by compression shear test can predict the strength behavior in a structural panel with a good accuracy, and on the other hand, the rolling shear modulus shows a conservative prediction compared with the value measured by bending shear tests.

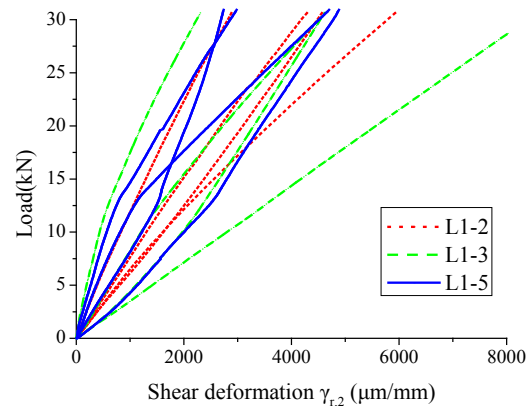


Figure 12: Shear deformation and load curve

4 Conclusion

For the determination of bending properties, the three-layer CLT panels made from Canadian hemlock showed representative testing results. Based on the bending tests of varied lengths of span, the bonding strength of the CLT panels between outer layers and cross-layers showed a relatively low level, which caused the failure of bonding lines in most cases. Rolling shear failure was another main failure mode, normally accompany with the bending failure or bonding line failure. Half of the bending specimens in group L1 showed a typical ductile failure mode, combining rolling shear and bending failures, while other specimens showed brittle failure modes. It indicated that Canadian hemlock CLT has a good potential for ductility and capability of energy dissipations.

According to the measuring results, the global MOE was gradually closer to the value of theoretical calculation with the increasing length of span. However, the local MOE performed inconsistently in different layouts, which indicated that the results obtained from group L1 were close to the theoretical value, and group L3 performed a lowest level.

The possible explanation is that more growing defects exist in the longer specimens, resulting in a relatively large deflection of the longer specimens, hence the value of local MOE decreases.

On the other hand, the new modified compression shear tests provided a relatively conservative value of the rolling shear strength and modulus, as the values were 1.28 MPa and 53.13 MPa, respectively. Compared with the compression shear tests, a high level of rolling shear strength and modulus (1.57 MPa and 234 MPa) of Canadian hemlock cross-layers was performed in the bending shear specimens possibly due to size effects of structural timber elements. It indicates that the compression shear test can accurately predict the rolling shear strength of Canadian hemlock CLT applied as structural elements, while the prediction of the rolling shear modulus by using this method is too conservative.

As a result, Canadian hemlock CLT panels with good bonding strength showed excellent bending strength, stiffness and an extent of ductility in bending tests. In order to enhance the bending property and to take the advantage of the rolling shear strength as much as possible, a better bonding quality or the edge bonding between elements in the cross-layer is recommended in CLT manufacturing. In addition, to determinate the rolling shear property of CLT panels, both the strain measurement in bending tests and the new modified compression shear test are feasible, and the latter one is more economical for the determination of the rolling shear strength.

Acknowledgement: This paper is funded by the Fundamental Research Funds for the Central Universities (22120180315), the Application for Collaborative Research Project under International Joint Research Laboratory of Earthquake Engineering (TMGFXK-2015-002-2) and Canada Wood Group financial support. And, Ningbo Sino-Canada Technology Research Institute is gratefully acknowledged for the CLT supplying.

References

Aicher, S.; Dill-Langer, G. (2000): Basic considerations to rolling shear modulus in wooden boards. *Otto-Graf-Journal*, vol. 11, no. 2000, pp. 157-165.

Aicher, S.; Hirsch, M.; Christian, Z. (2016): Hybrid cross-laminated timber plates with beech wood cross-layers. *Construction and Building Materials*, vol. 124, no. 2016, pp. 1007-1018.

ANSI/APA (2018): *PRG 320-2018: Standard for Performance-Rated Cross-Laminated Timber*. The Engineered Wood Association. Tacoma, WA, USA.

ASTM (2015): *ASTM D198-15: Standard Test Methods of Static Tests of Lumber in Structural Sizes*. American Society for Testing and Material, West Conshohocken, PA, USA.

ASTM (2011): *ASTM D2718-11: Standard Test Methods for Structural Panels in Planar Shear (Rolling Shear)*. American Society for Testing and Material, West Conshohocken, PA, USA.

Bendsten, B. A. (1976): Rolling shear characteristics of nine structural softwoods. *Forest Products Journal*, vol. 26, no. 11, pp. 51-56.

Blaß, H.; Görlacher, R. (2000): Rolling shear in structural bonded timber elements. *International Conference on Wood and Wood Fiber Composites*, vol. 5, pp. 1-5.

Blass, H. J.; Fellmoser, P. (2004): Design of solid wood panels with cross layers. *Proceeding of the 8th World Conference on Timber Engineering*, pp. 543-548.

CEN (2015): *EN 16351: 2015, Timber Structures-Cross Laminated Timber-Requirements*. European Committee for Standardization, CEN, Bruxelles, Belgium.

CEN (2018) *EN 1995-1-1: 2006+A1: 2018, Eurocode 5: Design of Timber Structures-Part 1-1. General-Common Rules and Rules for Buildings*. European Committee for Standardization, CEN, Bruxelles, Belgium.

CEN (2016): *EN 338: 2016. Structural Timber-Strength Classes*. European Committee for Standardization, CEN, Bruxelles, Belgium.

CEN (2012): *EN 408: 2010+A1: 2012: Structural timber and glued laminated timber-Determination of some physical and mechanical properties*. European Committee for Standardization, CEN, Bruxelles, Belgium.

CEN (2012): *EN 408: 2010+A1: 2012, Timber Structures-Structural Timber and Glued Laminated Timber-Determination of Some Physical and Mechanical Properties*. European Committee for Standardization, CEN, Bruxelles, Belgium.

Dauids, W. G.; Willey, N.; Lopez-Anido, R; Shaler, S.; Gardner D. et al. (2017): Structural performance of hybrid SPFs-LSL cross-laminated timber panels. *Construction and Building Materials*. vol. 149, no. 2017, pp. 156-163.

Ehrhart, T.; Brandner, R.; Schickhofer, G.; Frangi, A. (2015): Rolling shear properties of some European timber species with focus on cross laminated timber (CLT): test configuration and parameter study. *International Network on Timber Engineering Research: Proceeding of Meeting*, vol. 48, pp. 61-76.

Hindman, D. P.; Bouldin, J. C. (2015) Mechanical properties of southern pine cross-laminated timber. *Journal of Materials in Civil Engineering*, vol. 27, no. 9, 04014251.

Karacabeyli, E.; Douglas, B. (2013): *Cross-Laminated Timber Handbook*, U.S. ed. FPInnovations, Quebec, Canada.

Kreuzinger, H. (1999): Platten, Scheiben und Schalen-Ein Berechnungsmodell für gangige Statikprogramme (German). *Bauen mit Holz*, vol. 1, pp. 34-39.

Li, M. H. (2017): Evaluating rolling shear strength properties of cross-laminated timber by short-span bending tests and modified planar shear tests. *Journal of Wood Science*, vol. 63, no. 2017, pp. 331-337.

Li, Y. (2015): *Duration-of-load and Size Effects on the Rolling Shear Strength of Cross Laminated Timber (Ph.D. Thesis)*. University of British Columbia, Canada.

Madson, B.; Buchannan, A. H. (1986): Size effects in timber explained by a modified weakest link theory. *Canadian Journal of Civil Engineering*, vol. 13, no. 2, pp. 218-232.

Sikora, K. S.; McPolin, D. O.; Harte, A. M. (2016): Effects of the thickness of cross-laminated timber (CLT) panels made from Irish Sitka spruce on mechanical performance in bending and shear. *Construction and Building Materials*. vol. 116, no. 2016, pp. 141-150.

Steiger, R.; Gülzo, A.; Czaderski, C.; Howald, M. T.; Niemz, P. (2012): Comparison of bending stiffness of cross-laminated solid timber derived by modal analysis of full panels and by bending tests of strip-shaped specimens. *European Journal of Wood and Wood Products*. vol. 70, no. 2012, pp. 141-153.

Steiger, R.; Gülzow, A.; Gsell, D. (2008): Non destructive evaluation of elastic material properties of crosslaminated timber (CLT). *Proceeding of the Conference COST E53*, pp. 171-182.

Wang, Z. Q.; Fu, H. M.; Gong, M.; Luo, J. Y.; Dong, W. Q. et al. (2017): Planar shear and bending properties of hybrid CLT fabricated with lumber and LVL. *Construction and Building Materials*, vol. 151, no. 2017, pp. 172-177.

Zhou, Q. Y.; Gong, M.; Chui, Y. H.; Mohammad M. (2014): Measurement of rolling shear modulus and strength of cross-laminated timber using bending and two-plate shear tests. *Wood and Fiber Science*, vol. 46, no. 2, pp. 259-269.